Available online at www.sciencedirect.com

SciVerse ScienceDirect

Geochimica et Cosmochimica Acta 89 (2012) 116–133

Geochimica et Cosmochimica Acta

www.elsevier.com/locate/gca

# Carbon sequestration via reaction with basaltic rocks: Geochemical modeling and experimental results

Robert J. Rosenbauer [a,*], Burt Thomas [a], James L. Bischoff [a], James Palandri [b]

[a] U.S. Geological Survey, 345 Middlefield Road, Menlo Park, CA 94025, United States
[b] University of Oregon, Eugene, OR 97403, United States

Received 7 January 2011; accepted in revised form 20 April 2012

**Abstract**

Basaltic rocks are potential repositories for sequestering carbon dioxide ($CO_2$) because of their capacity for trapping $CO_2$ in carbonate minerals. We carried out a series of thermodynamic equilibrium models and high pressure experiments, reacting basalt with $CO_2$-charged fluids over a range of conditions from 50 to 200 °C at 300 bar. Results indicate basalt has a high reactivity to $CO_2$ acidified brine. Carbon dioxide is taken up from solution at all temperatures from 50 to 200 °C, 300 bar, but the maximum extent and rate of reaction occurs at 100 °C, 300 bar. Reaction path simulations utilizing the geochemical modeling program CHILLER predicted an equilibrium carbonate alteration assemblage of calcite, magnesite, and siderite, but the only secondary carbonate identified in the experiments was a ferroan magnesite. The amount of uptake at 100 °C, 300 bar ranged from 8% by weight for a typical tholeite to 26% for a picrite. The actual amount of $CO_2$ uptake and extent of rock alteration coincides directly with the magnesium content of the rock suggesting that overall reaction extent is controlled by bulk basalt Mg content. In terms of sequestering $CO_2$, an average basaltic MgO content of 8% is equivalent to $2.6 \times 10^8$ metric ton $CO_2/km^3$ basalt.
Published by Elsevier Ltd.

## 1. INTRODUCTION

There is broad scientific consensus that global warming and the resulting climate changes are caused by anthropogenic emissions of $CO_2$ (IPCC, 2007). Carbon dioxide capture and storage (CCS) is a major component of a portfolio of advanced energy technologies required to mediate the rise in concentration of atmospheric $CO_2$. In particular, sequestration of $CO_2$ as geochemically stable solid carbonates of Ca, Mg, and Fe through reaction with basaltic rocks has been tendered as a possible permanent sink for $CO_2$ (Seifritz, 1990; McGrail et al., 2006; Alfredsson et al., 2008; Oelkers et al., 2008; Gislason et al., 2009; Goldberg et al., 2009; Shikazono et al., 2009; Schaef et al., 2010). Immense basalt provinces exist worldwide in: Iceland, Hawaii, the Columbia River Plateau and India's Deccan Volcanic Province (McGrail et al., 2006; Prasad et al., 2009). Moreover, most basaltic flow complexes comprise multiple layers of flow tops that are macroporous and fracture-permeable and therefore contain significant pore capacity for storage of $CO_2$ fluid or carbonate reaction products (McGrail et al., 2006; Goldberg et al., 2008). Importantly, in regions lacking traditional sedimentary reservoirs, $CO_2$ injection into basalts may provide one of the only alternatives for geologic sequestration of $CO_2$.

Understanding the fundamental reactions of $CO_2$ with basalt is ever more important as the investment increases in pilot-scale sequestration projects. Similar reactions are also important in the evolution of geothermal projects in basalt that propose the use $CO_2$ as the working fluid (Pruess, 2006). Recent injection studies have been conducted in Iceland basalts and in the Palisades diabase of New York in which carbonated waters are injected into basaltic aquifers at depth (Matter et al., 2007; Alfredsson et al., 2008; Gislason et al., 2009). Under these conditions, and

* Corresponding author.
*E-mail address:* brosenbauer@usgs.gov (R.J. Rosenbauer).

0016-7037/$ - see front matter Published by Elsevier Ltd.
http://dx.doi.org/10.1016/j.gca.2012.04.042

as predicted by reaction-path modeling and experiments (Gysi and Stefansson, 2008, 2009), demonstrable mineral carbonation is expected.

## 2. PREVIOUS WORK

The literature related to carbon sequestration via mineral carbonation is dominated by aqueous phase studies of pure mineral reactions analogous to natural mineral weathering processes. Giammar et al. (2005) carried out batch experiments in stainless-steel acid-digestion bombs simultaneously reacting forsterite with water and with a separate supercritical $CO_2$ phase at pressures up to 104 bars and up to 95 °C. After 26 days forsterite dissolution did not result in magnesite precipitation even though conditions of mineral supersaturation were achieved. Bearat et al. (2006) reacted olivine with aqueous solutions and supercritical $CO_2$ under a variety of conditions and found optimum formation of secondary magnesite within an aqueous solution at 185 °C and 135 bar $pCO_2$. Gerdemann et al. (2007) reacted olivine under similar conditions using a continuously stirred autoclave. They found 85% conversion of olivine to magnesite within 6 h. Jones et al. (2010) reacted olivine at slightly higher temperature (200 °C) and found $Fe^{2+}$ was incorporated into carbonates more rapidly than $Fe^{2+}$ oxidation (and concomitant $H_2$ formation) leading to diminished yields of magnetite, $H_2$, and $H_2$-dependent $CH_4$ production. McGrail et al. (2006) reacted basalt with water and supercritical $CO_2$ at 90 °C and 100 bar $pCO_2$ and observed secondary calcite surface coatings. In similar experiments at 50 °C and 103 bars $pCO_2$, McGrail et al. (2009) suspended hand samples of basaltic rock within the supercritical, but water-saturated $CO_2$ phase above the water level. They observed secondary carbonate formation on the basalt after 95 days. However, the solubility of water in the supercritical $CO_2$ phase can be substantial; for instance, at 100 °C and 300 bars water solubility is approximately 2 mol% (Sabirzyanov et al., 2003; Schaef and Mcgrail, 2009; Spycher et al., 2003). Schaef et al. (2010) reacted basalts from various provinces at 100 °C, 103 bars in static autoclaves. They observed a large variation in weathering from "minor" to "severe" after up to one-year duration. Interestingly, they found no convincing correlation between reactivity and bulk composition.

Here, we report the use of geochemical model simulations and high-pressure experimental reactions among basalt, brine, and aqueous $CO_2$ over a range of temperatures, designed to probe the controls on the extent and rates of reaction between $CO_2$ and basaltic rock. This work aids in the identification of the important parameters controlling reaction extent and the determination of optimal geochemical conditions for the carbonation of basalt and mineral sequestration of $CO_2$. Model simulations were used to identify likely conditions of interest and a suite of subsequent experiments were designed to test important variables in reactions including the fluid saturations state with respect to $CO_2$, reaction temperature, and the bulk characteristics of the rocks that control reaction extent.

## 3. METHODS

### 3.1. Modeling methods

Thermodynamic equilibrium simulations were performed using CHILLER (Reed, 1982), which calculates the distribution of chemical components among minerals, gases, and species in the aqueous phase. The sources of most of the thermodynamic data, the methods of computing activity and fugacity coefficients, and an overview of the limitations of the method are discussed in Palandri and Reed (2004) and are not repeated here. The thermodynamic data for minerals and $H_2O$ and $CO_2$ gases, including supercritical $CO_2$, are derived from the data of Holland and Powell (1998). In these simulations the fluid was first equilibrated with basalt at the stated conditions, then $CO_2$ added incrementally and equilibrium recalculated at each step, to obtain the results discussed below.

Equilibrium constants for individual reactions of interest were calculated also utilizing SUPCRT (Johnson et al., 1992). Distributions of aqueous species and mineral saturation indices for the experimental data were computed using SOLMINEQ (Kharaka et al., 1988).

## 4. EXPERIMENTAL METHODS

### 4.1. Apparatus and experimental procedures

Experimental and analytical procedures generally followed the scheme described in Rosenbauer et al. (1983) with some modification for the injection, sampling and analysis of $CO_2$ (Rosenbauer et al., 2005). Liquid $CO_2$ was injected into the reaction vessel via syringe pumps (ISCO Corp./Teledyne Inc., Model D100) charged from a commercial $CO_2$ cylinder (Matheson Gas Inc.) equipped with a full-length eductor tube for liquid withdrawal. Briefly, most experiments were carried out in flexible Au–Ti reaction cells with ~200–350 $cm^3$ total volume, equipped with a small bore (2.3 mm) ¼ in. OD, Ti capillary exit tube and sampling valve. Serial sampling is therefore possible while maintaining constant pressure conditions in the reactor. The cell was contained within a chrome-vanadium autoclave that was secured within a cyclic rotating (180°) furnace (Rosenbauer et al., 1993). Before use, aqueous fluids were sparged for 2 h with $N_2$ to remove dissolved $O_2$. After the reactants were sealed inside the cell, the autoclave was pressurized to ~100 bar by adding water to the annulus surrounding the reaction cell inside the autoclave. The $CO_2$ was injected with a syringe pump and the assembly was heated to experimental temperature. Pressure was re-adjusted to target conditions and held constant while heating. Temperature was maintained by a proportional controller (Omega, Love™ Controls, Model 49) and measured with a type K thermocouple calibrated to a platinum resistance temperature detector (RTD). Pressure was measured with dead-weight calibrated analog gauges and digital transducers (Heise Corp.). In experiments where the solution is $CO_2$ saturated a small excess supercritical $CO_2$ phase is present. Constant agitation of these experiments ensures

that the fine-grained basalt was likely dominantly suspended in the aqueous phase.

At the conclusion of an experiment during cooling and depressurization, $CO_2$ was bled off from the reaction cell in concert with the withdrawal of water from the autoclave to preserve the integrity of the reaction cell. The autoclave and reaction cell were disassembled, and the reacted solids were filtered under a vacuum through 2.5 μ paper filters then dried overnight at 80 °C. The quench, reactor disassembly, and filtration were conducted within a period of less than one hour. The total quench volume and mass of reacted solids were determined.

### 4.2. Experimental design

Experiments were carried out at 50, 100, and 200 °C and from 100 to 300 bars, and at partial pressures of $CO_2$ simulating both $CO_2$-undersaturated and $CO_2$-saturated aqueous solutions (Table 1). Initial water/rock ratios were 10:1–2:1, representing approximately 200 g fluid and 20 or 100 g rock, varying in actual amount depending in cell volume. Initial water/liquid $CO_2$ volume ratios were ~2:1 to 20:1 in $CO_2$ saturated experiments. Fluid withdrawal during sampling had a negligible effect on water:rock ratios by the end of experiments (approximate 10% decrease in total fluid volume). After reaching steady-state based on aqueous chemistry, select experiments were conducted by instantaneously changing PT conditions or by re-injecting $CO_2$. In experiment designated 04-04, $CO_2$ was re-injected into the gold reaction cell to achieve a dissolved concentration of 1.0 M after the initial amount of $CO_2$ (1.0 M) had decreased to steady-state of less than 1.0 mM). In experiment designated 04-05, the initial temperature of 200 °C was lowered to 50 °C after steady-state to observe changes in fluid composition along a temperature gradient. We also conducted two long-term experiments in the gold cells held constant at 50 and 100 °C wherein the focus was on both the early changes in the aqueous chemistry and final equilibrium composition under supercritical $CO_2$ conditions (Duan and Sun, 2003). These experiments were sampled frequently in the beginning of each experiment then again after 4000 h.

A third set of three long-term batch experiments (09-01, 09-02, 10-08) with basalts of different composition were carried out in fixed-volume (200 ml), titanium-lined steel reaction vessels for the purpose of investigating only mineralogical changes and the net amount of $CO_2$ uptake by basalt. After the rock powder and fluids were loaded into the vessel, enough $CO_2$ was injected via a titanium capillary to achieve target pressure at temperature and to attain a final prescribed rock:fluid ratio. The vessel was then secured to a rotating furnace and heated to conditions. All titanium surfaces were passivated at 450 °C for 24 h before use. These experiments were carried out at 100 °C, 300 bar with initial (water or $scCO_2$): rock ratios of 10:1 and with an approximate water:liquid $CO_2$ ratio of 1:1 (Table 1). Fluid chemistry was not obtained for these experiments. The reacted solids were treated as above. $CO_2$ consumption during the experiments is expected to affect the total pressure only negligibly due to the large excess of $CO_2$.

### 4.3. Initial reactants and alteration products

Two different tholeitic basalts were utilized in experiments; A mid-ocean ridge basalt (MORB) from dredge haul L11-81-WF-17-40 on the Juan de Fuca Ridge (Dixon et al., 1986) designated JDF and a tholeite from Mt. Lassen (sample LC84-569) (Mertzman, 1977; Bacon et al., 1997; Grove et al., 2002; Clynne et al., 2008; Clynne and Muffler, 2010) designated MTL. In addition, a picrite (olivine basalt) was utilized in one long-term fixed volume experiment. The picrite is an olivine-rich tholeite from Houalalai Volcano. The groundmass is fine clinopyroxene, plagioclase, and Fe–Ti oxides, but about 50% of the rock is large olivine phenocrysts (Moore and Clague, 1992. These samples represent likely repository basalts for expected future injection in locations. Basalt reactants were crushed, sieved between 100 and 200 mesh, washed in distilled water and air-dried. The JDF tholeite used in the gold vessel experiments was coated in a glassy rind. This glassy rind was avoided when sampling the crystalline interior prior to crushing. The surface area of the powered JDF tholeite was determined by the BET method for both reactants and alteration products following experiments. The mineralogy of the tholeitic basalts comprises dominant calcic plagioclase, feldspar, and pyroxene with significant olivine (Table 3) as estimated by calculated idealized normative mineralogy. The picrite contained 50% olivine and significant plagioclase (Table 3). Before alteration major oxides were analyzed by atomic emission spectroscopy and FeO by dissolution and titration (Table 4) and after alteration $CO_2$ was determined by either coulometry (UIC Coulometrics™) and combustion/IR (SGS Mineral Services (Xral), Toronto, Canada). Solutions of sodium chloride (0.5 and 1.0 M) were prepared from

Table 1
Experimental conditions.

| Experiment number | Rock type | Temperature (°C) | Pressure (bar) | Water/rock | $CO_2$ (molal) | NaCl (molal) | Reaction vessel |
|---|---|---|---|---|---|---|---|
| 04-04 | JDF | 100 | 300 | 2:1 | 1.0 | 1.0 | Gold |
| 04-05 | JDF | 200/50 | 300 | 2:1 | 1.0 | 1.0 | Gold |
| 08-11 | JDF | 100 | 300 | 10:1 | SC | 0.5 | Gold |
| 08-12 | JDF | 50 | 300 | 10:1 | SC | 0.5 | Gold |
| 09-01 | Picrite | 100 | 300 | 10:1 | SC | 0.5 | Titanium |
| 09-02 | MTL | 100 | 300 | 10:1 | SC | 0.5 | Titanium |
| 10-08 | MTL | 100 | 300 | 10:1 | SC | 0.5 | Titanium |

SC, supercritical; JDF, Juan De Fuca; MTL, Mt. Lassen.

reagent grade NaCl and deionized-distilled water and analyzed for major impurities. The use of these two different NaCl concentrations for subsequent experiments is unfortunate but is not expected or intended to be an important variable for the interpretation of results.

## 5. ANALYTICAL METHODS

Periodically, except for the long-term fixed-volume Ti vessel experiments, aqueous samples were withdrawn from each experiment and analyzed for total dissolved inorganic carbon as above and dissolved cations by inductively coupled plasma using both atomic emission and mass spectroscopy (ICP-AES, ICP-MS), and dissolved anions except chloride by ion-chromatography, chloride ion was determined by potentiometric titration via a chloridometer (Labconco, Model 4425000). Serial samples were at intervals of a few hours or daily near the beginning of each experiment, then at increasingly longer intervals depending on perceived reaction rates and an estimate of nearness to steady-state concentrations for major cations. Total dissolved carbon ($C_t$) and pH were analyzed immediately after sampling on separate 0.5 ml samples. Reported pH values are maxima because the fluid samples began degassing $CO_2$ during sampling. The in situ carbonate species distribution and pH were calculated from $C_t$ and pH measured at 22 °C using the computer code SOLMINEQ (Kharaka et al., 1988). Refractive index was determined by a hand-held refractometer (Vista Vision) on a drop of fluid during each sampling event to measure total dissolved solids and to monitor the integrity of the reaction cell. Aliquots for major elements were syringe filtered (0.2 μm), diluted, and preserved for batch analyses. Quench fluids were analyzed immediately for pH and aliquots preserved for major element analyses. Dried-homogenized sub-samples of the reacted solids were analyzed for $CO_2$ by coulometry.

For the fixed volume Ti vessel batch experiments both the original and residual solids were analyzed by XRD to identify primary minerals, and by scanning electron microscopy (SEM) with energy dispersive spectroscopy (SEM/EDS) to obtain backscatter images and semi-quantitative mineral chemical compositions. Subsamples of solids for SEM/EDS analyses were mounted on ~1.2 cm diameter sample holders, affixed with double-sided carbon impregnated tape, and then coated with gold. Less than 5% of the solids were analyzed by SEM/EDS. The composition of the solids was determined by total dissolution and ICP-AES analysis (Xral Corporation).

## 6. RESULTS

### 6.1. Model results

Model simulations utilizing the computer program CHILLER were carried out at each of the experimental conditions but we highlight here the results in detail for the experiments carried out at 100 °C and 300 bar due to the maximum basalt reactivity at these conditions. In particular we compare the modeled results to the results of experiment 04-04, under-saturated with $CO_2$ wherein $CO_2$ was re-injected. In the simulations, NaCl (1.0 m) is first equilibrated with JDF basalt at pressure (300 bar) then temperature (100 °C), followed by an incremental addition of $CO_2$ (Fig. 1). Equilibrium is computed after each increment of $CO_2$ added to the system. The precipitation of dolomite and ankerite were intentionally suppressed in the model due to their known kinetic inhibitions. Otherwise, at high $pCO_2$, the model predicts that calcite dissolves and that both Mg and Ca precipitate as dolomite. A separate model simulation without these suppressed compositions is presented in Fig. 2. Here the primary carbonate phases are dolomite, siderite, and ankerite. As will be discussed subsequently, the primary observed carbonate mineral assemblage in all experiments is magnesite – supporting the model simulations that suppress dolomite and ankerite formation.

The model shows how the relative content of the mineral equilibrium assemblage changes with the addition of $CO_2$ (Fig. 1, upper 2 panels). The carbonates are shown separately in panel 3. The model predicts that calcite is the first and only carbonate to precipitate until about 40 g of $CO_2$ are added to the system (Fig. 1, panel 3). Dissolved cations remain relatively constant until about 30 g of $CO_2$ are added to the system (Fig 1; panel 4). The model also predicts that at final equilibrium most of the solid Fe is found in siderite with some in nontronite.

### 6.2. Experimental results

#### *6.2.1. 100 °C – $CO_2$-undersaturated gold-cell experiment with $CO_2$ reinjection, water:rock (JDF) = 2:1 (Expt: 04-04)*

All fluid geochemical cation data are presented in Table 2. Aqueous $CO_2$ decreased rapidly from 1.0 to ~0.1 M within the first 500 h of the experiment, then decreased asymptotically to 0.04 M at 2000 h duration (Fig. 3). Major dissolved cations (Ca, Mg, Fe) increased rapidly from below detection to maximum values within 24–72 h then, except for Mg, decreased by greater than a factor of 5 within another 96 h (Fig. 3). Fe and Mn continued to decrease asymptotically whereas dissolved Ca concentrations more than doubled from a minimum of 0.40 to 0.87 mM prior to re-injection of $CO_2$. In contrast, after dissolved Mg reached a maximum concentration of 37.0 mM at 72 h, the Mg concentration decreased gradually to 12.0 mM. Following re-injection of $CO_2$ at 2064 h, aqueous $CO_2$ again decreased rapidly from 0.5 to ~0.2 M then more slowly to 0.13 m by 2884 h. The major dissolved cations and metals followed a similar pattern. These components initially spiked in concentration, then decreased to near pre-injection levels (Fig. 3). The pH measured at ambient conditions (22 °C, 1 bar) was little changed over the course of the experiment, rising from and initial pH of 5.62 to 6.27 after 168 h duration. The pH measurements of early samples were typically 0.5 pH units higher than initial sample measurements but this effect became unimportant as $CO_2$ concentrations declined. Refractive index increased and decreased in concert with dissolved constituents.

#### *6.2.2. 200 and 50 °C – $CO_2$-undersaturated gold-cell experiment with abrupt temperature change, water:rock (JDF) = 2:1 (Expt: 04-05)*

Aqueous $CO_2$ decreased rapidly from 1.0 to ~0.6 M within the first 24 h of the experiment then stabilized at a

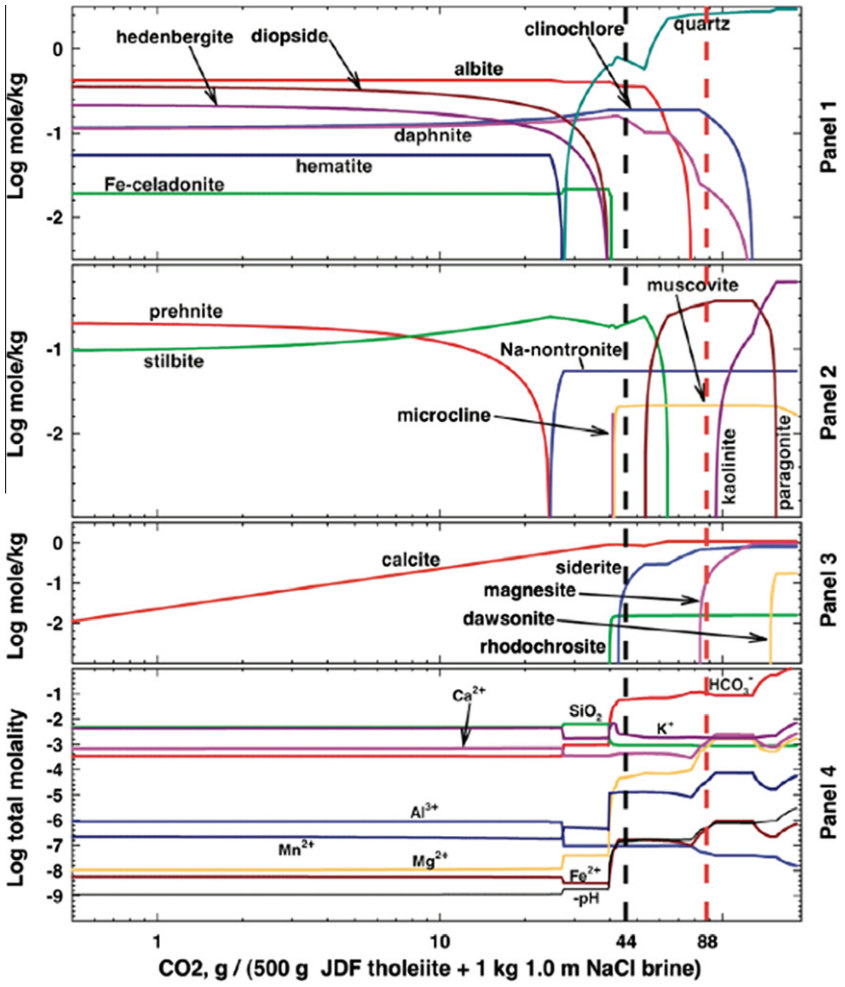


Fig. 1. Model simulation for experiment 04-04 (100 °C, 300 bar) utilizing the computer program CHILLER. In the simulation, NaCl (1.0 m) is first equilibrated with JDF basalt at pressure (300 bar) then temperature (100 °C), followed by an incremental addition of $CO_2$. Equilibrium is computed after each increment of $CO_2$ added to the system. Changes in mineralogy (panels 1–3) and aqueous chemistry (panel 4) are a function of $CO_2$ added. The vertical line at 44 g is the initial amount of $CO_2$; the vertical line 88 g is the cumulative amount of $CO_2$ added to the experiment. Note that the simulation predicts calcite and siderite as the dominant alteration carbonates with significant magnesite. Dolomite and ankerite were intentionally suppressed. Molality is used for simplicity in all model calculations, whereas experimentally derived quantities are expressed in molarity.

steady state concentration of 0.5 M prior to 96 h (Fig. 4). Dissolved $CO_2$ increased slightly after 900 h in concert with an unintended 13% drop in pressure from 300 to ~260 bar. Dissolved Ca increased rapidly to >5 mM within 24 h, then more slowly to 10 mM at 1080 h (Fig. 4). The concentration of Mg increased to 4.1 mM and remained constant (Fig. 4). The pH, measured at 22 °C, remained relatively constant at $5.78 \pm 0.04$. At 1080 h the temperature of the experiment was decreased to 50 °C to test the effect of temperature on equilibrium state concentrations. This new temperature condition was sampled 70 h following the temperature drop; dissolved $CO_2$ began a continuous decline for the remaining 1000 h duration of the experiment (Fig. 4). Both dissolved Ca and Mg doubled in concentration to 19.7 and 9 mM, respectively. Dissolved Ca asymptotically decreased following an initial increase falling to 0.12 mM 600 h after the temperature change; however, Mg began an asymptotic increase to a steady state value near 102.8 mM. Both dissolved Fe and Mn (not shown) changed after the temperature perturbation: Fe increased 15-fold from 0.18 to 2.8 mM before returning to 0.18 mM (Fig. 4); Mn also increased from 0.18 μM to 0.18 mM before decreasing back to 1.8 μM. The ambient-measured pH changed from a steady-state value of 5.8 at 200 °C to 6.2 immediately after the temperature shift and continued to rise to 6.8 by the end of the experiment.

#### *6.2.3. 100 °C – $CO_2$ saturated gold-cell experiment, water:rock (JDF) = 10:1 (Expt: 08-11)*

Dissolved constituents were monitored in the early stages of a multi-phase (solid, $CO_2$-saturated aqueous solution, excess supercritical $CO_2$) experiment until about 300 h then not again until nearly 4400 h. Dissolved Ca and Mg again displayed opposing trends. Dissolved Ca reached a peak concentration of 0.7 mM within the first hour of the experiment and subsequently decreased rapidly to a minimum of 0.4 mM

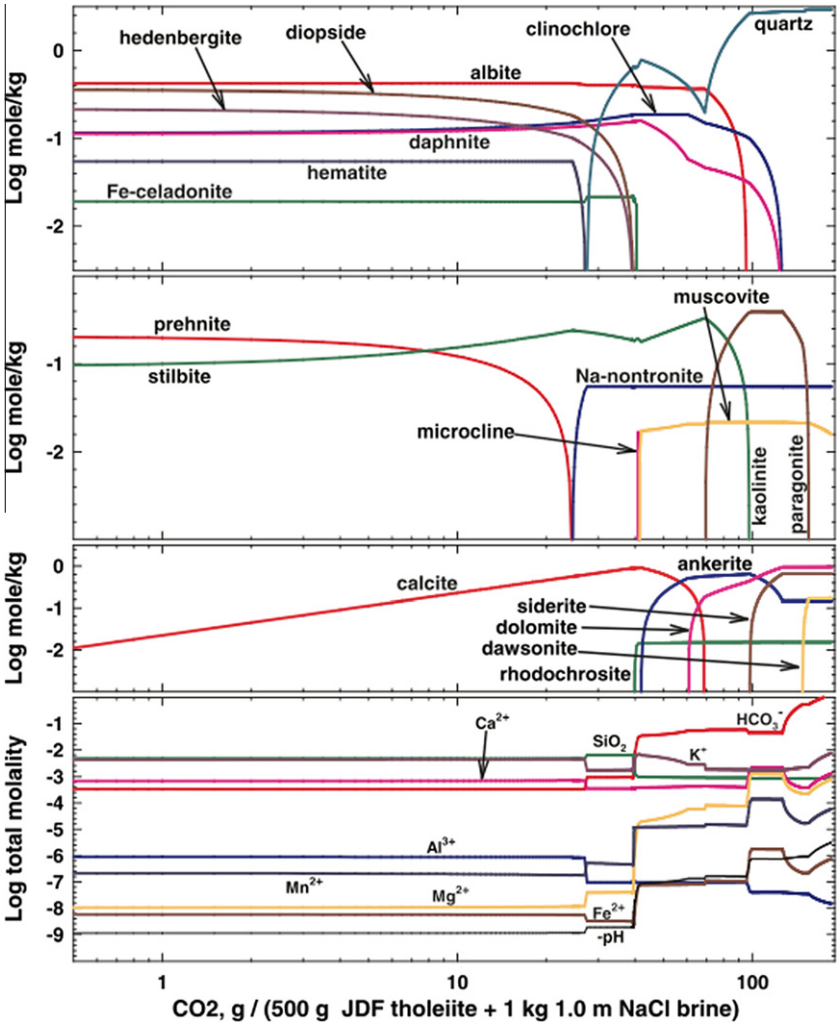


Fig. 2. Model simulation for experiment 04-04 without suppression of ankerite and dolomite.

at 100 h, then increased to a maximum final concentration of 0.9 mM at 4400 h (Fig. 5a). Dissolved Mg increased to a maximum of 38 mM within 83 h, then decreased slowly to a final concentration of 18 mM at 4400 h (Fig. 5b) absent a later increase as seen in Ca concentration. Dissolved $C_T$ remained constant at ~1.15 M. The ambient-measured pH increased from an initial value of 5.6 to a final value of 6.2.

*6.2.4. 50 °C – $CO_2$ saturated gold-cell experiment, water:rock (JDF) = 10:1 (Expt: 08-12)*

Experiment 08-12, conducted at 50 °C, is directly comparable to experiment 08-11 with a similar sampling approach and the presence of a separate excess supercritical $CO_2$ phase. Following an initial release of Ca and Mg from the rock to solution, both species decreased to minimum values within an hour after which both gradually increased in concentration over the next 300 h (Fig. 6a and b). Dissolved Mg continued to increase to a maximum of 59 mM whereas Ca reached a maximum concentration of 0.8 mM then decreased to near its minimum value after 4300 h. After an initial rapid increase, dissolved Fe and Mn continued to increase gradually to maximum values around 300 h before ultimately decreasing to minimum values after 4100 h (Fig. 6c and d). Dissolved $C_T$ remained constant at 1.3 m. The ambient-measured pH increased from an initial value of 5.7 to a final value of 6.5.

*6.2.5. 100 °C, 300 bar – Ti fixed volume vessel $CO_2$ saturated batch experiment, water:rock (MTL/picrite) = 10:1, water:$CO_2$ = 1:1*

The MTL tholeiite reacted with 0.5 M NaCl and supercritical $CO_2$ in two duplicate experiments at 100 °C and 300 bar for two months, took up 7.5 and 7.6 wt.% $CO_2$, respectively (Table 5). In contrast, olivine basalt (picrite), reacted under the same conditions and duration took up 26% $CO_2$ (Table 5).

The altered basalt from all fixed volume experiments was friable, to the eye appeared little changed from the original, and was easily poured from the vessel as slurry. Chemical analyses (Table 5) indicated that the altered basalt contained variable amounts of $CO_2$, representing fixed carbonate. XRD analysis indicated major ferroan magnesite ((Mg, Fe)$CO_3$) with moderate amounts of plagioclase, pyroxene, and quartz. The limit of detection by XRD is ~5%. SEM

Table 2
Experimental data.

| Experiment | Duration (h) | $CO_2$ (mM) | Ca (mM) | Mg (mM) | Fe (mM) |
|---|---|---|---|---|---|
| 04-04 | 0 | 673 | 2.3 | 3.0 | 0.17 |
| | 24 | 723 | 5.3 | 8.7 | 0.48 |
| | 72 | 593 | 1.7 | 36.8 | 0.52 |
| | 168 | 364 | 0.5 | 36.2 | 0.17 |
| | 216 | 270 | 0.4 | 32.5 | 0.14 |
| | 336 | 164 | 0.5 | 22.0 | 0.09 |
| | 408 | 141 | 0.5 | 19.4 | 0.08 |
| | 648 | 116 | 0.5 | 17.9 | 0.08 |
| | 720 | 91 | 0.5 | 17.6 | 0.07 |
| | 840 | 70 | 0.5 | 16.6 | 0.07 |
| | 1080 | 59 | 0.6 | 15.4 | 0.06 |
| | 1200 | 55 | 0.7 | 14.3 | 0.05 |
| | 1536 | 48 | 0.7 | 12.7 | 0.05 |
| | 1896 | 42 | 0.9 | 12.9 | 0.05 |
| | 2064 | 42 | 0.9 | 12.1 | 0.05 |
| $CO_2$ injection | 2065 | 468 | 0.6 | 29.0 | 0.33 |
| | 2089 | 411 | 0.4 | 28.1 | 0.13 |
| | 2161 | 334 | 0.4 | 27.9 | 0.13 |
| | 2233 | 261 | 0.5 | 24.9 | 0.13 |
| | 2353 | 226 | 0.7 | 23.3 | 0.12 |
| | 2569 | 188 | 1.0 | 22.2 | 0.11 |
| | 2689 | 184 | 1.2 | 21.1 | 0.11 |
| | 2881 | 161 | 1.5 | 19.7 | 0.11 |
| 04-05 | 0 | 673 | 3.0 | 0.0 | 0.01 |
| | 24 | 627 | 5.6 | 1.3 | 0.86 |
| | 96 | 504 | 8.5 | 4.4 | 0.22 |
| | 216 | 502 | 8.4 | 4.8 | 0.30 |
| | 552 | 504 | 9.0 | 4.0 | 0.17 |
| | 912 | 575 | 9.4 | 4.2 | 0.18 |
| | 1080 | 568 | 9.9 | 4.3 | 0.18 |
| $T = 50$ °C | 1368 | 559 | 19.7 | 9.0 | 2.78 |
| | 1392 | 579 | 18.9 | 15.3 | 4.63 |
| | 1416 | 564 | 19.2 | 24.6 | 4.41 |
| | 1440 | 575 | 18.1 | 39.0 | 2.54 |
| | 1584 | 470 | 3.5 | 89.5 | 0.30 |
| | 1704 | 423 | 0.5 | 99.7 | 0.17 |
| | 1896 | 370 | 0.1 | 99.9 | 0.18 |
| | 2112 | 323 | | | |
| | 2376 | 277 | | | |

| Experiment | Duration (h) | Ca (mM) | Mg (mM) | Fe (mM) | Mn (mM) |
|---|---|---|---|---|---|
| 08-11 | 0 | 0.68 | 2.19 | 5.16 | 0.88 |
| | 1 | 0.64 | 3.63 | 6.70 | 1.17 |
| | 12 | 0.71 | 6.45 | 4.81 | 0.70 |
| | 14 | 0.69 | 6.84 | 4.43 | 0.44 |
| | 24 | 0.65 | | 2.97 | 0.22 |
| | 38 | 0.60 | 33.6 | 0.48 | 0.06 |
| | 47 | 0.55 | 35.3 | 0.34 | 0.04 |
| | 83 | 0.42 | 38.4 | 0.25 | 0.04 |
| | 115 | 0.39 | 37.0 | 0.20 | 0.04 |
| | 258 | 0.41 | 32.9 | 0.18 | 0.03 |
| | 4362 | 0.91 | 17.7 | 0.09 | 0.002 |
| 08-12 | 0.2 | 0.71 | 18.69 | 1.12 | 0.01 |
| | 1.3 | 0.46 | 0.37 | 3.59 | 0.04 |
| | 14 | 0.57 | 0.44 | 3.65 | 0.05 |
| | 59 | 0.68 | 0.61 | 3.90 | 0.05 |
| | 92 | 0.75 | 0.69 | 4.03 | 0.06 |
| | 235 | 0.78 | 2.87 | 5.33 | 0.08 |
| | 4339 | 0.52 | 59.15 | 0.85 | 0.01 |

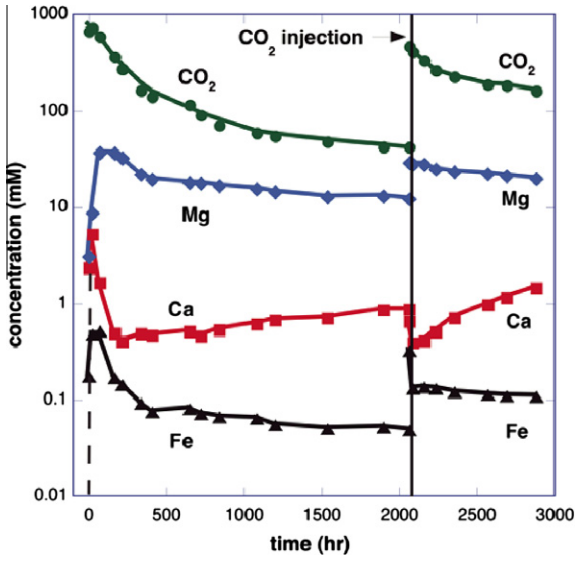


Fig. 3. Change in concentration of dissolved $CO_2$, Mg, Ca, and Fe in 1 m NaCl during reaction of $CO_2$ with tholeitic basalt (JDF) at 100 °C, 300 bar (Expt 04-04). Vertical line at 2064 h represents a re-injection of $CO_2$. Concentration is in mM/L; time is in hours; water/rock ratio equals two.

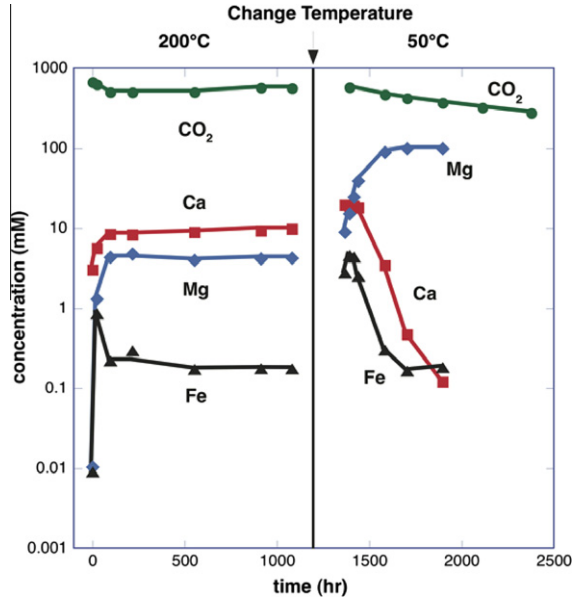


Fig. 4. Change in concentration of dissolved $CO_2$, Mg, Ca, and Fe in 1 m NaCl during reaction of $CO_2$ with tholeitic basalt (JDF) initially at 200 °C, 300 bar (Expt 04-05). Vertical line at 1080 h represents a change in temperature to 50 °C. Concentration is in mM/L; time is in hours; water/rock ratio equals two.

observation revealed abundant 1–4 μm rhombs of ferroan magnesite identified by SEM/EDAX and 2–5 μm botryoidal clumps of silica from the picrite experiment (Fig. 7). The alteration assemblage was the same for all experiments; only the amount of carbonate varied as indicated by $CO_2$ content (Table 5). The relative chemical composition of the altered basalt remained the same except for the addition of $CO_2$ that diluted the content of other components by the amount of uptake (Table 4). Chemical and mineralogical changes were greatest when reacting olivine basalt with $CO_2$. The rock accommodated 26 wt.% $CO_2$. This is equivalent to 85.2% of the divalent cations being incorporated into carbonate products (Table 5). The Mg equivalent calculated based upon the amount of $CO_2$ uptake (assuming magnesite precipitation) is roughly equal to the total amount of Mg available in the basalt (Table 6).

## 7. DISCUSSION

Experiments reacting basalt with $CO_2$-charged fluids, in both the presence and absence of a separate supercritical phase show that basalt is highly reactive to such fluids. In an aqueous system this reactivity is due to the dissolution of $CO_2$ in water to produce carbonic acid (1):

$$CO_2 + H_2O \leftrightarrow H_2CO_3 \quad (1)$$

a fundamentally important reaction because reactive hydrogen ion ($H^+$) produced by the dissociation of carbonic acid (2):

$$H_2CO_3 \leftrightarrow H^+ + HCO_3^- \quad (2)$$

potentially promotes mineral dissolution reactions (3):

$$4H^+ + Mg_2SiO_4 \leftrightarrow 2Mg^{2+} + SiO_2 + 2H_2O \quad (3)$$

The dissociation of carbonic acid is temperature dependent. There is a maximum in the $\log K$ of reaction (2) at ~50 °C above which $\log K$ decreases continuously with increasing temperature such that an initially weak acid becomes increasingly weaker at elevated temperature. Thus, at low temperatures, the increased availability of $H^+$ might be expected to lead to higher rates of wallrock hydrolysis. In the absence of any mineral reactions, and as a function of pressure, $CO_2$ dissolved in water produces an acidic solution of pH below 3 at typical geologic sequestration reservoir conditions (Toews et al., 1995). The addition of $CO_2$ to each of the present experiments conducted at 100 °C, lowered the ex situ measured pH from near neutral to less than 5.5 within the first 24 h, providing a source of reactive hydrogen ions. Previous experiments reacting basalt with NaCl solutions or seawater at similar and higher temperature conditions without a source of hydrogen ions produced negligible changes in fluid chemistry and no detectable alteration products (Seyfreid and Bischoff, 1979; Rosenbauer et al., 1983).

### 7.1. $CO_2$ under-saturated experiments

#### 7.1.1. $CO_2$ uptake

Based on changes in the fluid chemistry and XRD and SEM analyses of the experimental alteration products, divalent cations released from the basalt were precipitated as carbonates. The amount and rates of $CO_2$ uptake into secondary phases vary with temperature. We performed a mass balance calculation for experiment 04-04 taking into account the amount of $CO_2$ added to the experiment, the

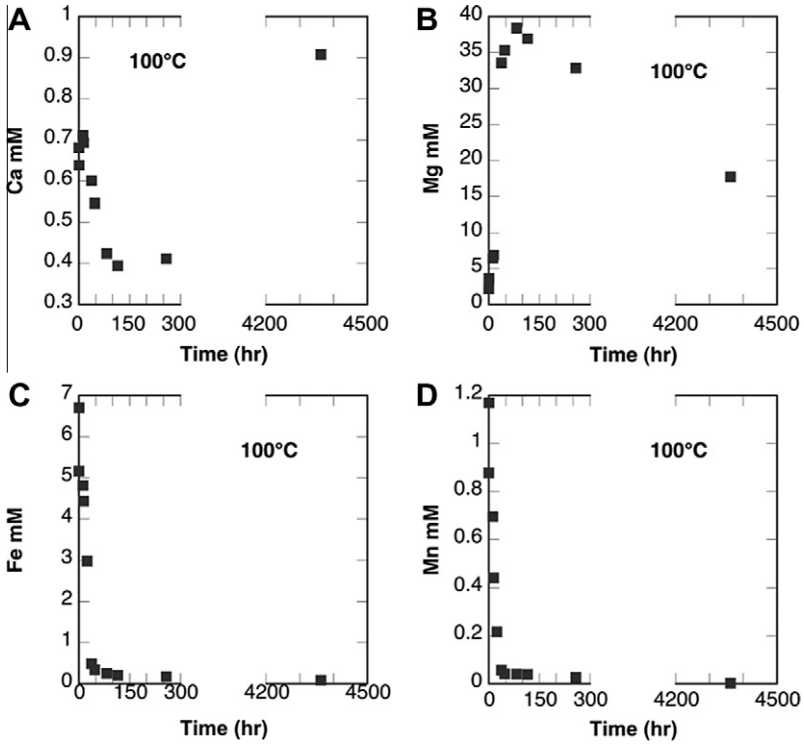


Fig. 5. Change in concentration of dissolved Ca (A), Mg (B), Fe (C), and Mn (D) in 0.5 m NaCl during reaction of $CO_2$ with tholeitic basalt (JDF) at 100 °C, 300 bar (Expt 08-11). Note the break in time between 300 and 4200 h. Concentration is in mM/L; time is in hours; water/rock ratio equals 10.

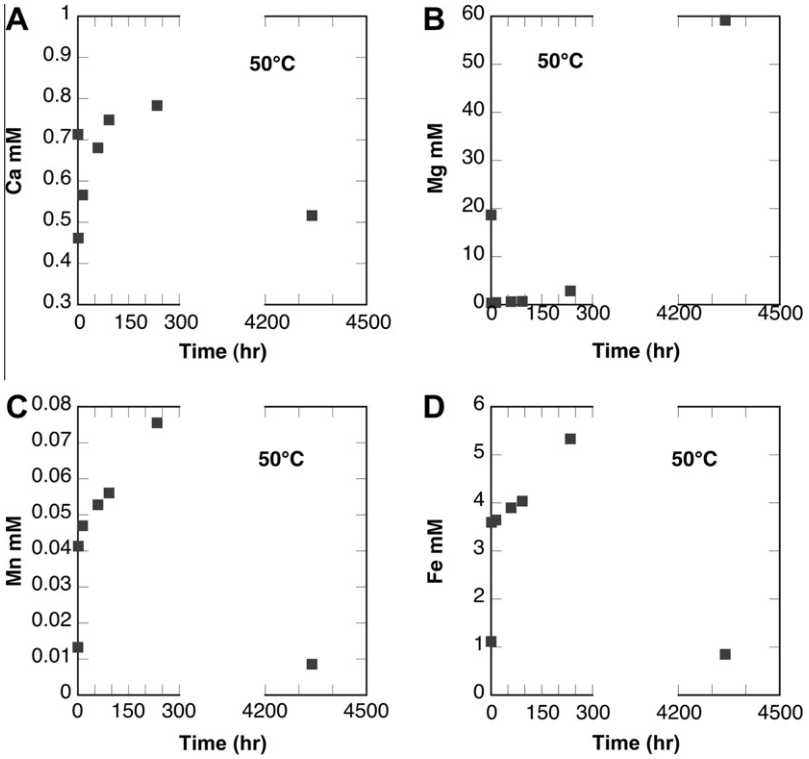


Fig. 6. Change in concentration of dissolved Ca (A), Mg (B), Fe (C), and Mn (D) in 0.5 m NaCl during reaction of $CO_2$ with tholeitic basalt (JDF) at 50 °C, 300 bar (Expt 08-12). Note the break in time between 300 and 4200 h. Concentration is in mM/L; time is in hours; water/rock ratio equals 10.

Table 3
Normative mineralogical compositions of tholeitic and olivine (picritic) basalt.

| | JDF (%) | Lassen | Picrite (%) |
|---|---|---|---|
| Orthoclase | 2.1 | 5.8 | 1.4 |
| Albite | 24.4 | 23.7 | 8.4 |
| Anorthite | 33.9 | 32.0 | 11.0 |
| Diopside | 14.8 | 16.3 | 9.2 |
| Hypersthene | 6.6 | | 13.8 |
| Olivine | 13.7 | 17.9 | 50.0 |
| Magnetite | 2.1 | 2.1 | 3.2 |
| Ilmenite | 1.9 | 1.9 | 1.7 |
| Apatite | 0.4 | 0.4 | 0.2 |
| Total | 100.2 | 100.1 | 98.9 |

Table 4
Chemical composition of tholeitic and olivine (picritic) basalt.

| Component | JDF tholeite (%) | Lassen tholeite (%) | Picrite (%) | Altered picrite (%) |
|---|---|---|---|---|
| $SiO_2$ | 49.1 | 49.6 | 44.5 | 32.6 |
| $Al_2O_3$ | 14 | 17.6 | 5.9 | 4.8 |
| $Fe_2O_3$ | 1.6 | 1.4 | 2.8 | 2.2 |
| FeO | 10.5 | 7.4 | 9.7 | 7.3 |
| MgO | 6.9 | 8.7 | 29.5 | 20.8 |
| CaO | 11.1 | 10.7 | 4.8 | 3.9 |
| $Na_2O$ | 2.4 | 1.6 | 1 | 0.8 |
| $K_2O$ | 0.2 | 1 | 0.2 | 0.1 |
| $P_2O_5$ | 0.2 | 0.2 | 0.1 | 0.8 |
| MnO | 0.2 | 0.1 | 0.2 | 0.1 |
| $CO_2$ | NA | 0.1 | 0.1 | 26.2 |
| $TiO_2$ | 0.99 | 0.99 | 0.89 | NA |
| LOI | NA | NA | 0.7 | NA |
| Total | 99.8 | 98.4 | 99.9 | 99.6 |

NA, not analyzed; LOI, loss on ignition.

Table 5
Alteration chemistry of basalt reacted with $CO_2$: $CO_2$ uptake JDF: Juan de Fuca; picrite: olivine basalt.

| Basalt | $CO_2$ | $CO_2$ uptake (percent by weight) | | |
|---|---|---|---|---|
| | | 50 °C | 100 °C | 200 °C |
| JDF | Under-saturated | 1.9 | 8.0 | 1.5 |
| JDF | Saturated | 2.0 | 7.0 | |
| Lassen | Saturated | | 7.5 | |
| Lassen | Saturated | | 7.6 | |
| Picrite | Saturated | | 26.2 | |

amount withdrawn during sampling, and the amount remaining at the end of the experiment. This mass balance results in a carbon sequestration estimate of 7.8% $CO_2$ by mass. This is in good agreement with a chemical analysis of the alteration product that indicates 8% $CO_2$ uptake by mass (Table 5). The close agreement between calculated and measured uptake indicates effects due to the retrograde solubility of the carbonates during quenching of the experiment are likely negligible. Nearly the entire amount of $CO_2$ initially injected into experiment 04-04 was removed from solution via sequestration as carbonate. Seventy-one percent of the initial dissolved $CO_2$ was removed from solution within the first 250 h at an average rate of ~0.005 mM/min. Based on the initial surface area of the solid phase of 0.565 $m^2/g$, the rate of removal was $1.3 \times 10^{-7}$ $M/m^2/g$. An additional 16% was removed over the course of the next 1600 h at decreasing rates as the concentration of $CO_2$ asymptotically approached zero. The $CO_2$ re-injected at 2000 h was removed at a significantly slower rate of 0.002 mM/min and appeared to asymptotically decrease to an equilibrium solution concentration (0.13 m) greater than the last concentration (0.04 m) measured before re-injection of $CO_2$, consistent with an approach toward the capacity limits of the basalt or a change in the alteration assemblage. A total of 88% of the second injection of $CO_2$ was removed. This repeated pattern of $CO_2$ injection and rapid removal from solution illustrates the high reactivity of the basalt to $CO_2$ and the absence of significant armoring of grains by reaction products including carbonates and silica phases.

For a generic reaction (4),

$$mA + nB = C \tag{4}$$

a reaction rate can be defined by (5)

$$r = k[A]^m[B]^n \tag{5}$$

where $A$ and $B$ are in mol/L and the exponents, m and n are determined by stoichiometry.

For the net reaction of olivine mineral with $CO_2$, $2CO_2 + Mg_2SiO_4 \rightarrow 2Mg_2CO_3 + SiO_2$ it follows from Eq. (5) that

$$r = k[CO_2]^2 \tag{6}$$

For the initial 250 h of the experiment at 100 °C, the log concentration of $CO_2$ was a linear function of time ($r^2 = 0.996$), thus the reaction rate with respect to $CO_2$ followed first order reaction kinetics where the rate coefficient ($k$) = −0.0051 $h^{-1}$. Overall, during the first phase of $CO_2$ reaction before re-injection, a plot of $1/[CO_2]$ versus time followed a linear trend ($r^2 = 0.98$), thus, the reaction rate followed second order kinetics where $k = 0.0129$ L $mol^{-1}$ $h^{-1}$. After re-injection, there is again a linear fit of log $[CO_2]$ versus temperature ($r^2 = 0.99$), but the first order reaction coefficient with respect to $CO_2$ was lower: $k = 0.0033$ $h^{-1}$). Over the entire duration following re-injection the linear fit of $1/[CO_2]$ versus time was fair ($r^2 = 0.94$) with a second order reaction coefficient of 0.0048 L $mol^{-1}$ $h^{-1}$. With respect to Mg, since the dominant reaction product is a ferroan magnesite, the overall reaction rate from the time of maximum dissolved Mg concentration up to the time of $CO_2$ re-injection also seems to follow second order kinetics where $k = 0.027$ L $mol^{-1}$ $h^{-1}$ ($r^2 = 0.92$). Within the first 500 h of the experiment from the time of maximum concentration of dissolved Mg, the data are consistent with first order kinetics: $k = -0.0094$ $h^{-1}$ ($r^2 = 0.99$) with respect to Mg.

In contrast, in experiment 04-05 wherein the initial temperature of 200 °C was lowered to 50 °C partway through the experiment, the amount of $CO_2$ taken up by

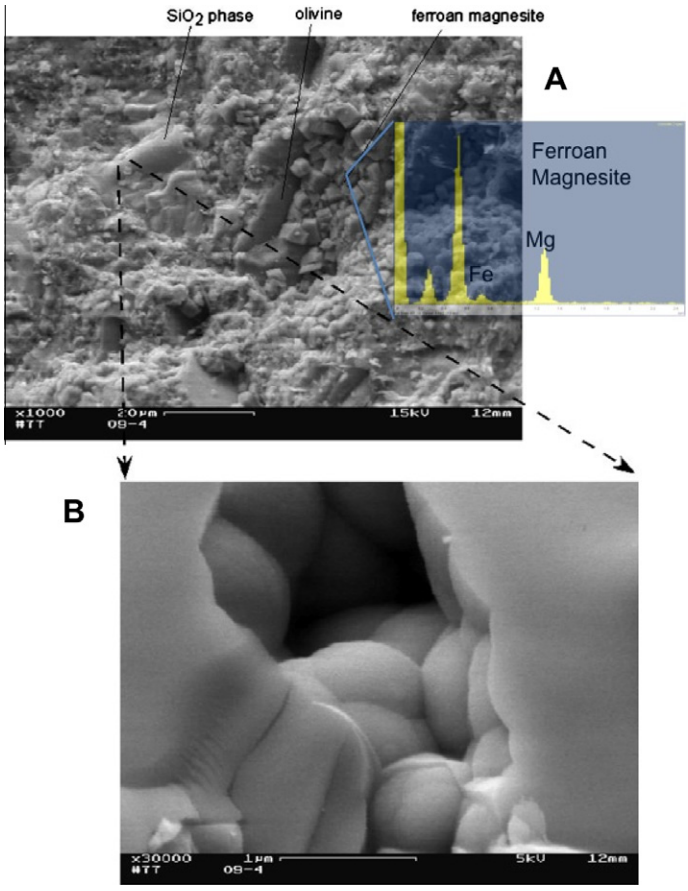


Fig. 7. Scanning electron microscope image of typical alteration assemblage of ferroan magnesite and botryoidal silica, from experiments reacting basalt with $CO_2$ in NaCl at 100 °C, 300 bar (Expt 09-01). The inset image is an SEM/EDAX analysis showing the dominant Mg content of the inferred ferroan magnesite carbonate phase.

Table 6
Alteration chemistry of basalt reacted with $CO_2$ at 100 °C 300 bar: Mg reacted. JDF: Juan de Fuca; picrite: olivine basalt.

| Basalt | $CO_2$ | $CO_2$ uptake (%) | Mg content un-reacted rock (mol) | Mg equivalent to $CO_2$ uptake (mol) |
|---|---|---|---|---|
| JDF | Under-saturated | 8.0 | 0.110 | 0.120 |
| JDF | Saturated | 7.0 | 0.039 | 0.037 |
| Lassen | Saturated | 7.5 | 0.030 | 0.031 |
| Lassen | Saturated | 7.6 | 0.031 | 0.031 |
| Picrite | Saturated | 26.2 | 0.130 | 0.110 |

basalt was only 1.5% at 200 °C and 1.9% at 50 °C, indicating that uptake of $CO_2$ at neither 200 °C nor 50 °C was as efficient as uptake at 100 °C. At 200 °C, the initial rate of $CO_2$ removal from solution was 0.005 mM/min, identical to the rate at 100 °C, but less $CO_2$ was removed (24%) at this temperature and steady-state was reached within a shorter time frame (96 h). Based on the initial surface area of the solid phase of 0.565 $m^2/g$, the rate of removal normalized to surface area was $1.1 \times 10^{-7}$ $M/m^2/g$ less than the rate $1.4 \times 10^{-7}$ $M/m^2/g$ observed at 100 °C. When the temperature was lowered to 50 °C, an additional 1.5% of $CO_2$ was removed from solution at a much lower initial rate of 0.0009 mM/min that continued to decrease with time. Forty-four percent of the $CO_2$ remaining at 200 °C was removed at 50 °C. At 200 °C, the experimental data are slightly better fit to first rather than zero order kinetics with respect to $CO_2$ (reaction (3)) where $k = -0.003\ h^{-1}$ ($r^2 = 0.99$). At 50 °C, the experimental data fit second order kinetics where $k = 6.6 \times 10^{-4}$ L $mol^{-1}$ $s^{-1}$ ($r^2 = 0.99$). Both the maximum rate and total amount of carbon uptake were highest at 100 °C. The least amount of uptake occurred at 200 °C. Previous experiments reacting rhyolite with $CO_2$ have also noted less alteration at higher temperature (Bischoff and Rosenbauer, 1996).

### 7.2. Aqueous chemistry

#### 7.2.1. Ca and Mg

At 100 °C, changes in the dissolved chemistry coincide with both injections of $CO_2$. The initial injection of $CO_2$ is

accompanied by spikes in the concentration of dissolved cations, notably Ca and Mg, likely in response to initial acidity due to the dissolution of $CO_2$ (Eq. (1)) and release of weakly bound ions on surfaces. Thermodynamic equilibrium modeling of the fluid chemistry, utilizing SOLMINEQ (Kharaka et al., 1988) indicates that the solution becomes supersaturated with respect to calcite, magnesite, and siderite, corresponding to three possible carbonate alteration phases for Ca, Mg, and Fe respectively. Saturation indices (log(ISP/KSP)) exceed 0 (Fig. 8a) when precipitation of these phases is thermodynamically favored. Saturation indices (SI) calculated for magnesite and siderite asymptotically approach the equilibrium line (log(ISP/KSP = 0)), consistent with the observation of ferroan magnesite as the major observed alteration product. However, the SI for calcite follows a similar decreasing temporal pattern that would suggest calcite is increasingly undersaturated following a brief initial supersaturation. The saturation index passes through the equilibrium condition log(ISP/KSP = 0) and achieves a steady-state SI value of −1.0. The slow increase in dissolved Ca over time and concomitant decrease in dissolved Mg following initial concentration spikes could be interpreted as an exchange of Mg for Ca from an early calcite precipitate or the transformation of an initially precipitated high calc magnesite or mixed Ca–Mg carbonate to magnesite. The absence of observed evidence of calcite is supported by the decrease in saturation state, despite the increase in dissolved Ca following the second injection of $CO_2$. If calcite were present in the alteration product, we would have expected some of it to dissolve with a corresponding increase in dissolved Ca after re-injection of $CO_2$ due to the increase of acidity accompanying the re-injection. In contrast dissolved Mg did increase as expected after injection, implying the carbonic acid promoted dissolution of a magnesite phase.

At 200 °C, the steady-state concentration of Ca is 10-fold higher and Mg 10-fold lower than at 100 °C. At 50 °C, again relative to the experimental data at 100 °C, dissolved Ca is 10-fold lower and Mg is 10-fold higher. These results are consistent with the retrograde solubility of magnesite. Other studies that have reacted basalt with seawater or heated seawater alone have also noted that the Ca/Mg ratio in solution increases with elevated temperature (Bischoff and Seyfreid, 1978; Seyfreid and Bischoff, 1979; Janecky and Seyfreid, 1983). When basalt is reacted with seawater at elevated temperature in the absence of supercritical $CO_2$, acidity is produced by the uptake of Mg from solution into smectite, in exchange for Ca (Seyfreid and Bischoff, 1979).

Evidence for Ca uptake in this study by precipitation of calcite is uncertain; no dolomite was observed. The positive correlation of Ca concentration with temperature does however imply that Ca resides in a solid phase. The spike in concentration following the decrease in temperature from 200 to 50 °C indicates a kinetically rapid dissolution of a solid phase, likely due to an increase in the dissociation of carbonic acid (2). Saturation indices (discussed below) indicate calcite remained supersaturated at 200 °C but re-attained equilibrium at 50 °C following dissolution of a calcium phase.

#### 7.2.2. Fe and Mn

Significant Fe and a lesser amount of Mn were initially released to solution at all temperatures except for Mn at 200 °C. At 100 °C, the changes in dissolved Mn occurred rapidly, reaching a maximum within 24 h (Fig. 5) and re-precipitating within 72 h. In contrast, the maximum in Fe concentration occurred at 72 h and slowly re-precipitated over the next 500 h more closely following the pattern of dissolved Mg, consistent with ferroan magnesite as the major alteration product. Following re-injection of $CO_2$ the concentration of dissolved Fe spiked, either in response to the acid dissolution of some ferroan magnesite or due to Fe-bearing phases remaining in the basalt. This Fe rapidly re-precipitated as the acid was neutralized by mineral reactions. Dissolved Mn increased then decreased only slightly after re-injection, an indication that the solid phase incorporating Mn was relatively pH insensitive. At 100 °C, there was a major shift toward higher total dissolved steady-state concentrations of $CO_2$, Mg, Ca, Fe, and Mn after re-injection of $CO_2$. The ambient-measured pH, both initially and after agitation to exsolve $CO_2$ was also higher by ~0.25 (initial) to ~0.7 (agitated) and may account for this shift. The change in temperature from 200 to 50 °C produced dramatic short-term spikes in both Fe and Mn but the final steady-state concentrations of Fe and Mn were similar at all temperatures.

#### 7.2.3. pH

Care was taken to measure pH immediately following sampling; however, $CO_2$ exsolution causes the pH measurements to drift upward; pH measured after physical sample agitation was typically 0.5 units higher on samples after $CO_2$ re-injection. Steady-state pH measured at 25 °C was dependent on the in situ experimental temperature, decreasing with increasing temperature from 6.75 (50 °C) to 5.75 (200 °C) owing to greater amounts of alkalinity production as the experiment progressed. Calculated in situ pH measurements range from 6.52 (50 °C) to 5.43 (200 °C).

#### 7.2.4. Mineral saturation indices

The uncertainty in pH measurement has a direct affect on the distribution of species calculated by SOLMINEQ and affects the calculation of saturation indices of mineral phases. For example, in the last sample from experiment 04-04 (100 °C) taken at 2881 h, a change of −1.0 pH units changes the calculated in situ pH from 6.09 to 5.13 and lowers the $HCO_3^-$ activity 4-fold from 0.046 to 0.012 and the saturation index of magnesite by −1.5. The saturation indices of calcite and siderite are likewise affected. The SOLMINEQ database does not contain ferroan magnesite but for experiment 04-04 at 100 °C, the saturation indices for magnesite and siderite closely coincide to within 0.2 units through a duration extending from 168 to 2060 h. This time period is prior to re-injection of $CO_2$ and these values asymptotically approach 0.0 as expected if the solution gradually approaches equilibrium with these phases. After re-injection of $CO_2$, the saturation indices for both siderite and magnesite again coincide and followed a similar temporal pattern. However, steady-state concentrations were apparent at one

order of magnitude super-saturated (SI = 1). In contrast, following re-injection the solution appeared to be at equilibrium with respect to calcite. Interestingly, no calcite has been observed in the alteration products. Since calculated saturation indices are dependent on the measured pH from decompressed fluid, these saturation index discrepancies could be a result of pH measurements that are biased toward higher values. Perhaps not coincidently, the lower pH values for samples after re-injection of $CO_2$ improves from 3% to <1% the difference in the calculated electro-neutrality of the solution due to a re-speciation of dissolved carbonate.

At 200 °C, based on its SI, magnesite is the precipitating phase (Fig. 8b); both calcite and siderite remained super-saturated. Following the temperature drop to 50 °C, the solution approaches equilibrium with calcite and becomes super-saturated with respect to both siderite and magnesite by 2 orders of magnitude. The only secondary phase detectable by SEM and XRD was ferroan magnesite, similar to the reaction product produced at 100 °C.

### 7.3. $CO_2$ saturated experiments

#### 7.3.1. $CO_2$ uptake

Because of an excess of $CO_2$ in a separate supercritical phase, the concentration of total dissolved $CO_2$ is dependent on its solubility and thus remained constant at 1.2 m at 100 °C and 1.3 m at 50 °C and did not yield information on $CO_2$ uptake. Examination of the solids after these experiments showed that the basalt had taken up 7% and 2% $CO_2$ at 100 and 50 °C after 6 months duration. Although carried out at different water/rock ratios and saturation states of $CO_2$, the amounts of $CO_2$ taken up by basalt in the presence of a separate supercritical phase were very similar to the amounts taken up in the under-saturated $CO_2$ experiments at 100 °C (~8%), 200 °C (~2%), and 50 °C (~2%). These results imply that the amount of basalt in the experiment at 100 °C had neared its capacity to sequester $CO_2$ after the second injection of $CO_2$ and may explain the elevated steady-state concentration of $CO_2$ post injec-

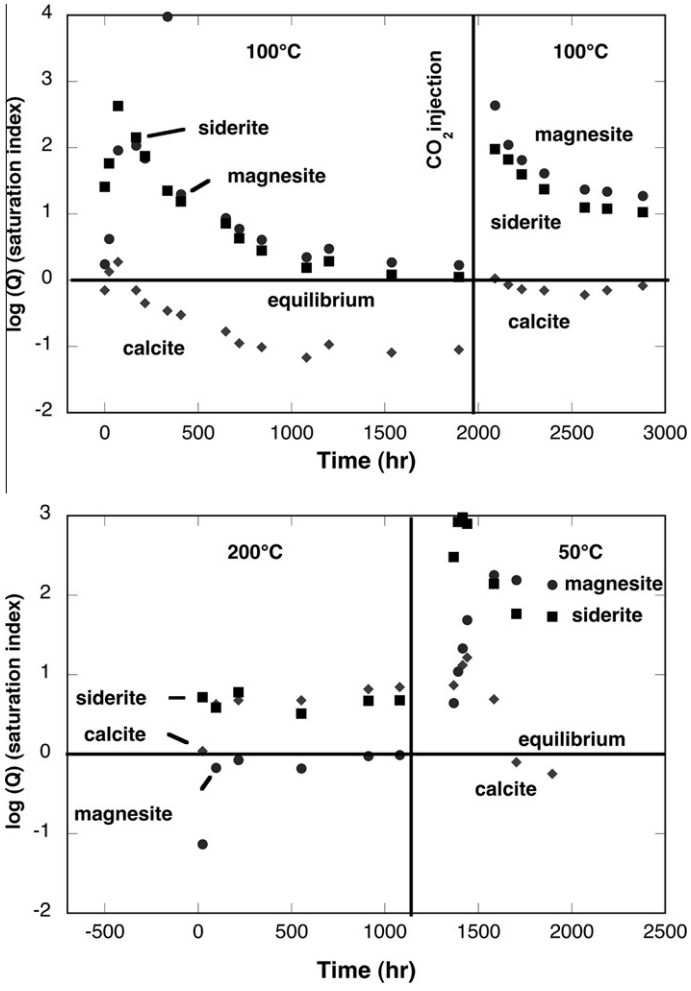


Fig. 8. (A) Change in saturation indices for siderite, magnesite, and calcite calculated using SOLMINEQ92 and the solution chemistry during reaction of $CO_2$ in 1 m NaCl with tholeitic basalt at 100 °C, 300 bar. The equilibrium line is defined by log (IAP/KSP) = 0. Positive values indicate the mineral is supersaturated, favoring precipitation; negative values indicate the mineral is undersaturated, favoring dissolution. Re-injection of $CO_2$ into the experiment occurred at 2064 h (vertical line). Water:rock ratio equals two. (B) Change in saturation indices for siderite, magnesite, and calcite calculated using SOLMINEQ92 and the solution chemistry during reaction of $CO_2$ in 1 m NaCl with tholeitic basalt initially at 200 °C, 300 bar. Temperature was changed to 50 °C at 1080 h (vertical line).

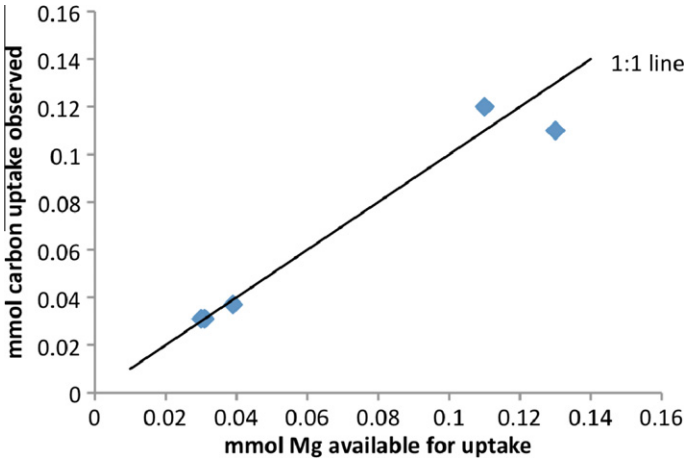


Fig. 9. The relationship between the available Mg in each of the experiments listed in Table 5 and the observed carbon uptake is depicted along with the 1:1 line implying Mg content may control reaction extent.

tion relative to the concentration prior to re-injection. At both 200 and 50 °C, the amount of dissolved $CO_2$ was not the limiting factor in determining $CO_2$ uptake.

The limiting factor may however, be the amount of Mg in the basalt. The quantity of $CO_2$ removed from solution at 100 °C in both the under-saturated and saturated experiments correlates well with the amount of Mg in the rock (Table 6). In the $CO_2$ under-saturated experiment 0.12 mol of $CO_2$ were removed from solution compared with 0.11 mol of Mg available in the amount of rock used in the experiment. In the $CO_2$ saturated experiment 0.037 mol of $CO_2$ removal compares with 0.039 mol of Mg in the amount of rock in this experiment. These results are comparable to the Ti-vessel batch experiments wherein Lassen tholeitic basalt took up 7.5 and 7.6% $CO_2$, equivalent to 0.030 and 0.031 mol compared to 0.031 mol of Mg in the rock (Table 6). The results are also consistent with the experimental alteration by supercritical $CO_2$ of olivine basalt (picrite) containing 0.13 mol Mg, wherein the rock took up 26% $CO_2$ equivalent to 0.11 mol (Table 6). The direct relationship between carbon uptake and Mg content in each of these experiments is depicted in Fig. 9.

### 7.4. Aqueous chemistry

#### *7.4.1. Ca and Mg*

The final steady-state concentrations of dissolved Ca and Mg coincided almost exactly between the saturated and under-saturated systems, except for dissolved Mg at 50 °C, suggesting that both components are controlled by similar alteration phases, independent of the amount of $CO_2$ available. Ferroan magnesite but not calcite nor other new Ca-bearing phases were observed in the alteration products from all experiments and likely controls dissolved Mg. In the absence of a discernable Ca phase, it is possible that magnesite contained some undetected Ca in addition to the observed Fe. The relatively high Mg content of the fluids may perhaps play a role in poisoning calcite crystal growth.

A comparison of the temporal patterns in the long-term $CO_2$ saturated experiments for both dissolved Ca and Mg show the trends are reversed for 50 and 100 °C and reversed for each component at the same temperature. At 100 °C, after some initial Ca dissolution from the rock, there is a decidedly concave pattern to the evolution of the fluid (Fig. 5a) versus a convex pattern for dissolved Mg (Fig. 5b). There is a minimum in dissolved Ca occurring at ~100 h coinciding with a maximum in dissolved Mg that could be interpreted the onset of a calcite to magnesite transition. This transition coincides also with the occurrence of steady-state for the SI calculated for magnesite (Fig. 10a), although at a value two orders of magnitude supersaturated. But, according to the SI for calcite, this solution was mostly under-saturated until the final data point, indicating equilibrium.

At 50 °C, the temporal trends are reversed: convex for Ca (Fig. 6a) with a maximum at 250 h and concave for Mg (Fig. 6b) with a minimum within an hour. Saturation indices for this fluid indicate that siderite remains super-saturated throughout, magnesite goes from under- to super-saturated, and calcite goes from under-saturated to near-saturation (Fig. 10b).

There is a clear temperature dependence to the concentrations of dissolved Ca and Mg when basalt is reacted with a constantly $CO_2$-saturated solution. The temporal patterns for dissolved Ca and Mg exhibit the same reversal in shape versus temperature for the same element as were evident between elements at the same temperature (Figs. 5a, b and 6a, b), ultimately leading to higher values of Ca at higher temperature compared to higher values of Mg at lower temperatures. Overall, from 50 to 200 °C, the Ca/Mg ratio increases exponentially (Fig. 11). This phenomenon has been noted elsewhere when basalt is reacted with seawater in the absence of $CO_2$ (Hardie, 1996). At elevated temperatures Mg partitions into solid phases. Even in the absence of basaltic rocks, heated seawater precipitates magnesium hydroxy sulfate (Bischoff and Seyfreid, 1978).

#### *7.4.2. Fe and Mn*

Substantially more (~10×) Fe and Mn were initially released to solution in the $CO_2$ saturated (10:1) water:rock

(W:R) versus the under-saturated (2:1) W/R experiments possibly reflecting a slightly lower initial pH. At 50 °C, the concentrations of Fe and Mn were comparable between the saturated and under-saturated experiments.

### 7.5. Model-experiment comparison

The composition of the physical experiment (04-04), at steady-state after the initial amount of $CO_2$ had reacted, corresponds to a point on Fig. 1 where 44 g of $CO_2$ have been added (black dashed line). At this point, total dissolved $CO_2$ and Ca in the experiment agree well with model predictions. But in the experiment, dissolved Mn is $\sim 10\times$ lower and Mg, and Fe are 100 and 1000 times higher, respectively than predicted by the model. Modeled Mn is in transition at 40 g of added $CO_2$, being incorporated within rhodocrosite, a mineral phase not identified in the reaction products of the experiment. In lieu of magnesite, the model incorporated Mg into a clinochlore–daphnite solid solution. No clay minerals were observed among the reaction products of the experiments. The pH is more alkaline in the model compared to the experiment.

Steady-state in the experiment, after $CO_2$ was re-injected, corresponds to 88 g of $CO_2$ added to the model (red dashed line). Dissolved Mn is still $\sim$10 less and Fe is now 2 orders of magnitude more concentrated in the experiment compared to the model. Dissolved Mg is within an order of magnitude, $\sim$5 times more concentrated in the experiment. The pH is slightly more alkaline, +0.5, in the model compared to the experiment. Dissolved Si is 10 times more concentrated in the experiment, likely due to steady-state control by amorphous silica rather than modeled quartz. Again, for kinetic reasons amorphous silica appears in the experiments whereas in these model simulations quartz is the equilibrium phase. Theoretical equilibrium calculations performed with CHILLER do not account for absolute rates of mineral dissolution and precipitation.

In contrast to the experimental results wherein ferroan magnesite was identified as the only secondary phase, the model predicts the early formation of calcite that persists to the end, with only sub-equal amounts of siderite and magnesite.

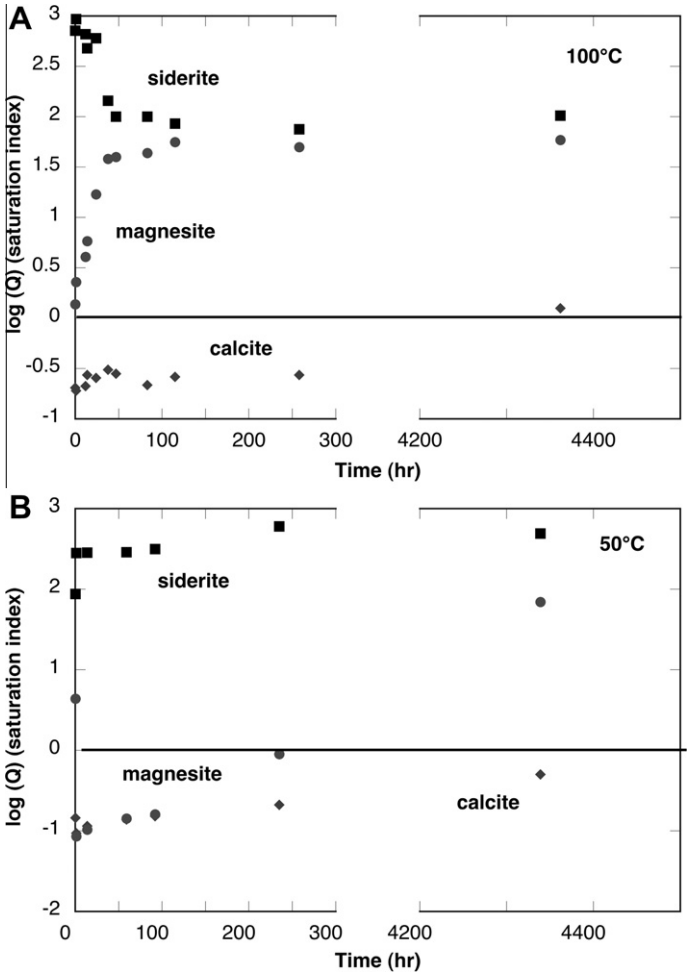


Fig. 10. (A) Change in saturation indices for siderite, magnesite, and calcite calculated using SOLMINEQ92 and the solution chemistry during reaction of $CO_2$ in 0.5 m NaCl with tholeitic basalt at 100 °C, 300 bar. The equilibrium line is defined by log (IAP/KSP) = 0. Positive values indicate the mineral is supersaturated, favoring precipitation; negative values indicate the mineral is undersaturated, favoring dissolution. Water/rock ratio equals 10. (B) Change in saturation indices for siderite, magnesite, and calcite calculated using SOLMINEQ92 and the solution chemistry during reaction of $CO_2$ in 0.5 m NaCl with tholeitic basalt at 50 °C, 300 bar.

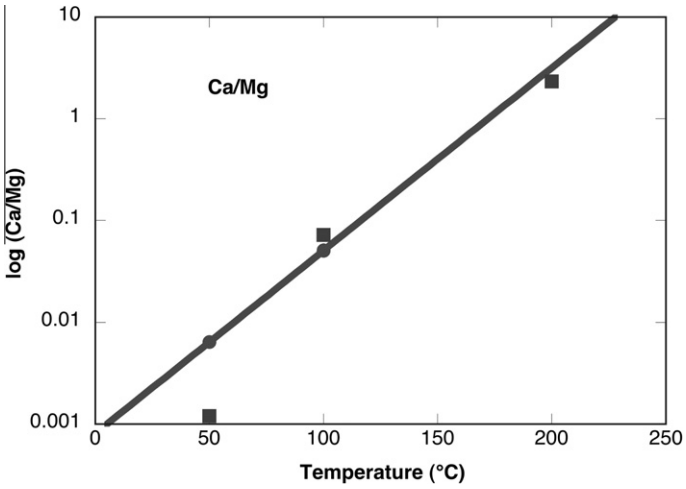


Fig. 11. Change in the dissolved Ca/Mg ratio versus temperature when tholeitic basalt reacts with $CO_2$ in 1 m NaCl at a W/R = 2 (solid squares) and in 0.5 m NaCl at a W/R = 10 (filled circles). The line is a best fit to the data from the 1 m NaCl experiment and extrapolated to the axes.

We originally utilized the modeling results to establish the optimal experimental conditions in the batch reactions at 100 °C wherein the amount of $CO_2$ added should have resulted in an alteration assemblage of calcite, siderite, and magnesite. These experiments also produced an alteration assemblage of ferroan magnesite and amorphous silica.

### 7.6. Implications for $CO_2$ sequestration

The results of these experiments, conducted under conditions likely to occur at ~3000 m injection sites in basaltic aquifers, show that basalt can convert supercritical $CO_2$ to stable carbonate minerals. The reactions appear to be optimal near common reservoir conditions (100 °C, 300 bar) but limited at higher temperatures than observed along a standard geothermal gradient (25 C/km). The diminished reactions at higher temperatures might be observed associated with enhanced geothermal reservoirs, however. Our results also suggest that the bulk chemistry of basalt determines the extent of reaction with $CO_2$. Specifically, the strong dependence of $CO_2$ uptake with Mg content is likely to prove a useful predictor of $CO_2$ uptake. At an average MgO content of 8%, the equivalent and maximum amount of $CO_2$ converted to magnesite is 0.087 $CO_2$ g/g basalt. Assuming an average basalt density of 3.0 g/cc the maximum uptake is ~0.26 g/cc or $2.6 \times 10^{11}$ kg/km$^3$, equivalent to $2.6 \times 10^8$ metric ton/km$^3$ basalt. If 1% of the rock were available for reaction, 2 years of an average power plant production of 1.2 million ton $CO_2$/year (IEA, 2010) could be accommodated in 1 km$^3$.

One important caveat to the above estimate relates to the experimental observations of dominant magnesite and amorphous silica reaction products despite geochemical equilibrium model expectations of dolomite, calcite, and quartz. Given these observed reaction products, the reaction of olivine to form magnesite (7):

$$Mg_2SiO_4 + 2H_2CO_3 = 2MgCO_3 + 2H_2O + SiO_2 \quad (7)$$

has a positive $\Delta V$ (Johnson et al., 1992) which would likely result in inhibition of injectability within deep Mg-rich basalts. Despite the proven capacity of these voluminous basalts to uptake $CO_2$ the feasibility of injection remains an important point for future research.

## 8. CONCLUSIONS

Basalt is highly reactive in the presence of $CO_2$-acidifed brine and the extent of reaction correlates with the Mg content of the bulk rock. $CO_2$ uptake occurs at 200 and 50 °C but both the extent and rate of reaction are greatest at 100 °C. Experiments at this temperature resulted in a net sequestration of approximately 8% and 26% $CO_2$ by mass in tholeite and picrite respectively. An average basaltic MgO content of 8% is equivalent to $2.6 \times 10^8$ metric ton $CO_2$/km$^3$ basalt. Ferroan magnesite is the dominant carbonate reaction product. Calcite was not observed in the alteration assemblage, in contrast to geochemical modeling that predicts calcite should precipitate.

## ACKNOWLEDGMENTS

We thank Tamer Koksalan and Junfeng Qin and for their invaluable laboratory assistance in setting up and sampling the experiments and Camille Jones, John Fitzpatrick, Jim Hein, and Natalie Johnson for their aid in the geochemical analyses. We thank also Bob Burruss and Yousif Kharaka for thoughtful and comprehensives reviews that greatly improved this manuscript.

## REFERENCES

Alfredsson H. A., Hardarson B. S., Franzson H. and Gislason S. R. (2008) $CO_2$ sequestration in basaltic rock at the Hellisheidi site in SW Iceland: stratigraphy and chemical composition of the rocks at the injection site. *Mineral. Mag.* **72**, 1–5.

Bacon C. R., Bruggman P. E., Christiansen R. L., Clynne M. A., Donnelly-Nolan J. M. and Hildreth W. (1997) Primitive

magmas at five cascade volcanic fields: melts from hot, heterogeneous sub-arc mantle. *Can. Mineral.* **35**, 397–423.

Bearat H., McKelvy M. J., Chizmeshya A. V. G., Gormley D., Nunez R., Carpenter R. W., Squires K. and Wolf G. H. (2006) Carbon sequestration via aqueous olivine mineral carbonation: role of passivating layer formation. *Environ. Sci. Technol.* **40**, 4802–4808.

Bischoff J. L. and Seyfreid W. E. (1978) Hydrothermal chemistry of seawater from 25 °C to 350 °C. *Am. J. Sci.* **278**, 838–860.

Bischoff J. L. and Rosenbauer R. J. (1996) The alteration of rhyolite in $CO_2$ charged water at 200 and 350 degrees C: the unreactivity of $CO_2$ at higher temperature. *Geochim. Cosmochim. Acta* **60**, 3859–3867.

Clynne M. A. and Muffler L. J. P. (2010) *Geologic map of Lassen Volcanic National Park and vicinity, California*. U.S. Geological Survey Scientific Investigations Map I-2899, Scale 1:50,000.

Clynne M. A., Muffler L. J. P., Siems D. F., Taggart, Jr. J. E. and Bruggman P. (2008). *Major and EDXRF trace element chemical analyses of volcanic rocks from Lassen Volcanic National Park and vicinity, California*. USGS Open-File, Report 2008-1091.

Dixon J. E., Clague D. A. and Eissen J. P. (1986) Gabbroic xenoliths and host ferrobasalt from the Southern Juan de Fuca ridge. *J. Geophys. Res. Solid Earth Planets* **91**, 3795–3820.

Duan Z. and Sun R. (2003) An improved model calculating $CO_2$ solubility in pure water and aqueous NaCl solutions from 273 to 533 K and from 0 to 2000 bar. *Chem. Geol.* **193**, 257–271.

Gerdemann S. J., O'Connor W. K., Dahlin D. C., Penner L. R. and Rush H. (2007) Ex situ aqueous mineral carbonation. *Environ. Sci. Technol.* **41**, 2587–2593.

Giammar D. E., Bruant R. G. and Peters C. A. (2005) Forsterite dissolution and magnesite precipitation at conditions relevant for deep saline aquifer storage and sequestration for carbon dioxide. *Chem. Geol.* **217**, 257–276.

Gislason S. R., Broecker W. S., Oelkers E. H., Gunnlaugsson E., Sigurdardottir H., Stefansson A., Wolff-Boenisch D., Matter J., Stute M. and Axelsson G. (2009) The carbfix project: mineral $CO_2$ sequestration into basalt. *Geochim. Cosmochim. Acta* **73**, A440.

Goldberg D. S., Takahashi T. and Slagle A. L. (2008) Carbon dioxide sequestration in deep-sea basalt. *Proc. Natl. Acad. Sci. USA* **105**, 9920–9925.

Goldberg D. S., Kent D. V. and Olson P. E. (2009) Potential on-shore and off-shore reservoirs for $CO_2$ sequestration in central Atlantic magmatic province basalts. *Proc. Natl. Acad. Sci. USA* **107**(4), 1327–1332.

Grove T. L., Parman S. W., Bowring S. A., Price R. C. and Baker M. B. (2002) The role of an $H_2O$-rich fluid component in the generation of primitive basaltic andesites and andesites from the Mt. Shasta region, N California. *Contrib. Miner. Petrol.* **142**, 375–396.

Gysi A. P. and Stefansson A. (2008) Numerical modeling of $CO_2$–water–basalt interaction. *Mineral. Mag.* **72**, 55–59.

Gysi A. P. and Stefansson A. (2009) $CO_2$–water–basalt interaction: geochemical modeling and experiments. *Geochim. Cosmochim. Acta* **73**, A483.

Hardie L. A. (1996) Secular variation in seawater chemistry: an explanation for the coupled secular variation in the mineralogies of marine limestones and potash evaporites over the past 600 my. *Geology* **24**, 279–283.

Holland T. J. B. and Powell R. (1998) An internally consistent thermodynamic data set for phases of petrological interest. *J. Metamorph. Geol.* **16**, 309–343.

IEA (2010) *$CO_2$ emissions from fuel combustion*. IEA Publication, ISBN: 978-92-64-08027-8.

IPCC (2007) *Climate Change 2007, the Fourth Assessment Report (AR4)*. UN Environment Program, Geneva.

Janecky D. R. and Seyfreid W. E. (1983) Solubility of magnesium hydroxysulfate hydrate at elevated temperature and pressure. *Am. J. Sci.* **283**, 831–880.

Johnson J. W., Oelkers E. H. and Helgeson H. C. (1992) Supcrt92 – a software package for calculating the standard molal thermodynamic properties of minerals, gases, aqueous species, and reactions from 1-bar to 5000-bar and 0-degrees-C to 1000-degrees-C. *Comput. Geosci.* **18**, 899–947.

Jones L. C., Rosenbauer R., Goldsmith J. I. and Oze C. (2010) Carbonate control of $H_2$ and $CH_4$ production in serpentinization systems at elevated P–Ts. *Geophys. Res. Lett.* **37**(37), L14306. http://dx.doi.org/10.1029/2010GL043769.

Kharaka Y. K., Gunter W. D., Aggarwal P. K., Perkins E. H. and DeBraal J. D. (1988) *Solmineq.88 a computer program for geochemical modeling of water–rock interactions*. U.S. Geological Survey water resources investigations report 88-4227.

Matter J., Takahashi T. and Goldberg D. (2007) Experimental evaluation of in situ $CO_2$–water–rock reactions during $CO_2$ injection in basaltic rocks: implications for geological $CO_2$ sequestration. *Geochem. Geophys. Geosyst.* **8**. http://dx.doi.org/10.1029/2006GC001427.

McGrail B. P., Schaef H. T., Ho A. M., Chien Y. J., Dooley J. J. and Davidson C. L. (2006) Potential for carbon dioxide sequestration in flood basalts. *J. Geophys. Res. Solid Earth* **111**, 1–13 (B12): Art. No. B12201, 1–13.

McGrail B. P., Schaef H. T., Glezakou V. A., Dang L. X. and Owen A. T. (2009) Water reactivity in the liquid and supercritical $CO_2$ phase: has half the story been neglected? *Energy Procedia* **1**, 3415–3419.

Mertzman S. A. (1977) The petrology and geochemistry of the medicine lake volcano. *Contrib. Miner. Petrol.* **62**(3), 221–247.

Moore J. G. and Clague D. A. (1992) Volcano growth and evolution of the island of Hawaii. *GSA Bull.* **104**, 1471–1484.

Oelkers E., Gislason S. R. and Matter J. (2008) Mineral carbonation of $CO_2$. *Elements* **4**, 333–337.

Palandri J. L. and Reed M. H. (2004) Geochemical models of metasomatism in ultramafic systems: serpentinization, rodingitization, and sea floor carbonate chimney precipitation. *Geochim. Cosmochim. Acta* **68**, 1115–1133.

Prasad P. S. R., Sarma D. S., Sudhakar L., Basavaraju U., Singh R. S., Begum Z., Archana K. B., Chavan C. D. and Charan S. N. (2009) Geological sequestration of carbon dioxide in Deccan basalts: preliminary laboratory study. *Curr. Sci.* **96**, 288–291.

Pruess K. (2006) Enhanced geothermal systems (egs) using $CO_2$ as working fluid – a novel approach for generating renewable energy with simultaneous sequestration of carbon. *Geothermics* **35**, 351–367.

Reed M. H. (1982) Calculation of multicomponent chemical equilibria and reaction processes in systems involving minerals, gases and an aqueous phase. *Geochim. Cosmochim. Acta* **46**(4), 513–528.

Rosenbauer R. J., Bischoff J. L. and Radtake A. S. (1983) Hydrothermal alteration of graywacke and basalt by 4 molal NaCl. *Econ. Geol.* **78**, 1701–1710.

Rosenbauer R. J., Bischoff J. L. and Potter J. M. (1993) A flexible Au–Ir cell with quick assembly for hydrothermal experiments. *Am. Mineral.* **78**, 1286–1289.

Rosenbauer R. J., Koksalan T. and Palandri J. L. (2005) Experimental investigation of $CO_2$–brine–rock interactions at elevated temperature and pressure: implications for $CO_2$ sequestration in deep-saline aquifers. *Fuel Process. Technol.* **86**, 1581–1597.

Sabirzyanov A. N., Shagiakhmetov R. A., Gabitov F. R., Tarzimanov A. A. and Gumerov F. M. (2003) Water solubility of carbon dioxide under supercritical and subcritical conditions. *Theor. Found. Chem. Eng.* **37**, 51–53.

Schaef H. T. and Mcgrail B. P. (2009) Dissolution of Columbia River basalt under mildly acidic conditions as a function of temperature: experimental results relevant to the geological sequestration of carbon dioxide. *Appl. Geochem.* **24**, 980–987.

Schaef H. T., Mcgrail B. P. and Owen A. T. (2010) Carbonate mineralization of volcanic province basalts. *Int. J. Greenhouse Gas Control* **4**, 249–261.

Seifritz W. (1990) $CO_2$ disposal by means of silicates. *Nature* **345**, 486.

Seyfreid W. E. and Bischoff J. L. (1979) Low temperature basalt alteration by seawater: an experimental study at 70 °C adn 150c. *Geochim. Cosmochim. Acta* **43**, 1937–1947.

Shikazono N., Harada H., Ikeda N. and Kashiwagi H. (2009) Dissolution of basaltic rocks and its application to underground sequestration of $CO_2$ – estimate of mineral trapping by dissolution–precipitation simulation. *Jpn. Mag. Mineral. Petrol. Sci.* **38**, 149–160.

Spycher N., Pruess K. and Ennis-King J. (2003) $CO_2$–$H_2O$ mixtures in the geological sequestration of $CO_2$. I. Assessment and calculation of mutual solubilities from 12 to 100 degrees C and up to 600 bar. *Geochim. Cosmochim. Acta* **67**, 3015–3031.

Toews K. L. and Shroll R. M., et al. (1995) pH-defining equilibrium between water and supercritical $CO_2$. Influence on SFE of organics and metal chelates. *Anal. Chem.* **67**, 4040–4043.

*Associate editor:* Jeffrey C. Alt